Full Length Article

# Modelling water table depth at rewetted peatlands with Sentinel-1 and Sentinel-2

Eoin Reddin [a,b] [iD],*, Jennifer Hanafin [b], Mingming Tong [c] [iD], Laurence Gill [d], Mark G. Healy [a]

[a] *Civil Engineering, University of Galway, Galway, H91 TK33, Ireland*
[b] *Irish Centre for High-End Computing, University of Galway, Galway, H91 TK33, Ireland*
[c] *Mechanical Engineering, University of Galway, Galway, H91 TK33, Ireland*
[d] *Department of Civil, Structural, and Environmental Engineering, Trinity College Dublin, Dublin, D02 PN40, Ireland*

## ARTICLE INFO

## ABSTRACT

Water table depth is the primary consideration during peatland rewetting, as a post-industrial peatland transitions from a degraded system with bare peat surfaces to a natural one. For rewetting to be successful, water table depth should be maintained in the upper 0.2 m of the soil to promote carbon sequestration while minimising net greenhouse gas emissions. There is evidence that satellite remote sensing techniques may be effective tools at monitoring water table depth. However, these techniques have been seldom used on degraded bare peat bogs, despite their excellent potential as monitoring tools during the restoration process. The aims of this paper are to (1) systematically test the relationship between radar backscatter and water table depth (2) compare decision tree regression algorithms to evaluate the potential of multi-sensor remote sensing in peatland management, and (3) make novel estimations of site-wide water table depth using a multi-sensor approach. This paper applies multi-sensor machine learning techniques to two post-industrial harvesting degraded peatlands, which are currently undergoing rewetting. Combined, these peatlands have nearly three years (2021–2023) of water table measurements, from over 50 piezometers. These data were used to train machine learning models, resulting in $R^2$ values ranging from 0.72 to 0.78, and RMSE values of 0.14 m and 0.12 m. Significant variation in water level throughout the year was observed, suggesting that the ability for a peatland to successfully sequester carbon may be temporally variable. With this study, we provide a timely assessment of restoration efforts at anthropologically degraded bare peat peatlands. This work proves the utility of remote sensing techniques in tracking restoration progress, and may inform future strategies in peatland restoration, rewetting, and monitoring.

## 1. Introduction

Wetland ecosystems cover approximately 5%–8% of Earth's land surface (Mitsch and Gosselink, 2007), and play a major role in the global greenhouse gas (GHG) cycle, exchanging significant amounts of carbon dioxide ($CO_2$) and methane ($CH_4$) (Evans et al., 2021). However, though effective $CO_2$ sinks, industrial peat-harvesting (primarily on raised peatlands) and burning has meant that these peatlands have recently acted as sources of GHG (Aitova et al., 2022). In their post-industrial "degraded" state, these peatlands are characterised by bare peat surfaces, low vegetation cover, and extensive groundwater drainage systems, but maintain the potential to be restored to a natural state (Mackin et al., 2017). "Re-wetting" is the process of undoing these drainage systems, so that the underlying water table depth (WTD) may be sufficiently raised. There are several strategies to rewet degraded bare peat peatlands, with the principle aim of maintaining WTD and

creating conditions compatible with *Sphagnum* growth (Mackin et al., 2017). Peat dams are routinely installed within excavated drains to raise the surrounding WTD (Worrall et al., 2007). Peat embankments (bunds) may be constructed to maintain standing water (Mackin et al., 2017). In cases where there has been extensive vegetation removal, introducing *Sphagnum* may initiate peat-formation — though this requires suitable pre-existing hydrological conditions (Quinty and Rochefort, 2003).

By rewetting and raising the WTD, peat regeneration may begin as peatlands revegetate (Price et al., 2023). *Sphagnum* moss and other vegetation grows on the peat surface and access moisture from the underlying water table through capillary action (Price et al., 2023). Regan et al. (2020) show that optimal WTD must be maintained within −0.2 m of the peat surface during restoration. Evans et al. (2021) further constrain this optimal range, finding that WTD between −0.05

---

**Table 1**

Previous studies comparing backscatter intensity and ground water, the relationship strength is measured by either Pearson's correlation coefficient (R), Spearman's correlation coefficient ($\rho$), or the $R^2$ value.[a, b] Relationship strength value given for Isoaho et al. (2024) and Räsänen et al. (2022) differ from those in Section 1.2, as here they refer exclusively to the relationship between backscatter intensity and ground water, rather than between multi-sensor indices and ground water.

| Author | Mission | Band–Polarisation | Relationship strength | Country | Ground type |
|---|---|---|---|---|---|
| Asmuß et al. (2019) | Sentinel-1 | C–VV/VH | $\rho$: 0.45 | Germany | Temperate Peatland |
| Bechtold et al. (2018) | ENVISAT | C–VV | R: 0.33–0.54 | Germany | Drained–Natural Peatland |
| Hrysiewicz et al. (2023) | Sentinel-1 | C–VV/VH | R: 0.17–0.76 | Ireland | Vegetated Raised Bog |
| Isoaho et al. (2024)[a] | Sentinel-1 | C–VV/VH | $R^2$: 0.32 | Finland | Restored Boreal Peatland |
| Kasischke et al. (2003) | ERS-2 | C–VV | $R^2$: 0.05–0.78 | USA | Florida Everglades |
| Kasischke et al. (2009) | ERS-2 | C–VV | R: −0.84–0.74 | USA | Boreal Wetland |
| Kim et al. (2017) | Radarsat-1/ALOS | C/L–HH/HV | $R^2$: 0.67–0.76 | USA | Great Dismal Swamp |
| Lang and Kasischke (2008) | ENVISAT | C–HH/VV | $R^2$: 0.19–0.5 | USA | Forested Wetland |
| Lees et al. (2021) | Sentinel-1 | C–VV | R: 0.77 | UK | Vegetated Peatland |
| Millard and Richardson (2018) | Radarsat-2 | C–HH/HV/VV | $R^2$: 0.11–0.66 | Canada | Mixed-Vegetation Peatland |
| Räsänen et al. (2022)[b] | Sentinel-1 | C–VV/VH | $R^2$: 0.21–0.34 | Finland | Mixed-Vegetation Peatland |
| Sass and Creed (2008) | ERS | C–VV | $R^2$: 0.45 | Canada | Boreal Peatland |
| Zhang et al. (2022) | Sentinel-1 | C–VV/VH | $R^2$: >0.5 | Florida | Florida Everglades |

to −0.13 m results in net GHG sequestration ($CO_2$ and $CH_4$). WTD outside of this range results in net GHG emissions (Evans et al., 2021). Therefore, water table monitoring and maintenance is of fundamental importance during the restoration process. Typically, this is carried out using piezometers to take in-situ measurements (Monteverde et al., 2022), though these can be laborious and time-consuming to install and maintain, and they only provide measurements of WTD near the instrument. Additionally, peatlands may be challenging environments to perform ground-based analyses. They can have little to no established pathways, and may contain waterlogged soil that is difficult to traverse, either on-foot or by machinery. As such, in-situ measurements may be complemented by satellite-based remote sensing, which facilitates site-wide observation, at various spatial resolutions at regular temporal intervals (Bhatnagar et al., 2020; Hrysiewicz et al., 2023). However, current Synthetic Aperture Radar (SAR) and optical satellite missions do not allow for direct measurement of WTD. Some studies have identified correlations between radar backscatter intensity and WTD (e.g. Bechtold et al. (2018) and Lees et al. (2021)), while others have used multi-sensor observations and machine learning techniques to estimate site-wide WTD (Räsänen et al., 2022; Isoaho et al., 2024). These multi-sensor techniques show good potential as a predictive tool to complement piezometer measurements. However, to date, such methods have not been applied to monitor the restoration of extraction-driven degraded bare peat peatlands, and their potential in this context is not understood. Therefore, this paper aims to apply multi-sensor (Sentinel-1 and Sentinel-2) machine learning techniques to degraded bare peat peatlands, to estimate site-wide WTD. As peatland restoration measures are introduced nationally and internationally across Europe, measuring WTD is of critical importance to assess the restoration progress. The approach presented here allows for WTD monitoring at a large scale, allowing for continuous monitoring of peatland rewetting strategies.

## 1.1. Monitoring peatland water table depth using synthetic aperture radar

The application of Synthetic Aperture Radar in environmental science, and peatland monitoring in particular, is a burgeoning field. The wealth of data provided by Sentinel-1 allows for observation of entire peatlands at regular intervals (6–12 days, depending on the number of satellites in constellation). SAR platforms allow for all-weather, year-round imaging of the Earth's surface. Sentinel-1 transmits in the C-band, in both Vertical-Vertical (VV) and Vertical-Horizontal (VH) polarisations. Following an acquisition, the radar information is presented as a Single Look Complex (SLC) image. SLC pixels comprise complex numbers of radar phase and intensity. The radar phase is a measure of the two-way distance between the satellite and ground surface, while intensity is a measure of the strength of the returned signal. Radar phase has been used in peatlands to measure "bog breathing" (cycles of uplift and subsidence driven by seasonal fluctuations in

soil moisture) (Hrysiewicz et al., 2023, 2024), while the relationship between backscatter intensity and soil moisture has been observed by several satellites (ENVISAT, ERS, Sentinel-1, ALOS, Radarsat) in various polarisations (VV, VH, HH, HV), across several wetland environments (Table 1). Correlation coefficients have varied from 0.17–0.77, while $R^2$ (coefficient of determination) values have varied between 0.05–0.78 (Table 1). From these studies, it is clear that there is some relationship between radar backscatter intensity and water level in peatlands. However, the peatlands studied in Table 1 vary significantly in terms of vegetation cover, latitude, and land-use. Previous studies (e.g. Bechtold et al. (2018) and Lees et al. (2021)) have improved the strength of the relationship between backscatter intensity and WTD by using environmental variables to filter SAR data. Wagner et al. (1999) showed that vegetation dynamics and soil moisture affect radar backscatter. Similarly, several studies have applied corrections to backscatter data in order to mitigate the impact of vegetation on backscatter. Bechtold et al. (2018) used the cross-cover angles method (Wagner et al., 1999), while Lees et al. (2021) and Räsänen et al. (2022) applied incidence angle and sine corrections to their data. Lees et al. (2021) found that these corrections improve the correlation coefficient between backscatter and WTD by 8.6% and 48.5%, respectively.

In a vegetated environment, the radar backscatter intensity ($\sigma_t^0$) can be expressed by Eq. (1) (Wang et al., 1995). Here, $\sigma_t^0$ is given by the sum of backscatter from the ground surface ($\sigma_s^0$), volume scattering through the vegetation canopy ($\sigma_c^0$), canopy–ground scattering ($\sigma_m^0$), and double bounce scattering between the ground surface and trunks ($\sigma_d^0$).

$$\sigma_t^0 = \sigma_s^0 + \sigma_c^0 + \sigma_m^0 + \sigma_d^0 \qquad (1)$$

$\sigma_s^0$ is primarily affected by surface roughness and the dielectric soil properties (controlled by soil moisture). Therefore, soil moisture variation with WTD will affect these dielectric properties and $\sigma_s^0$. This change in $\sigma_s^0$ will affect $\sigma_t^0$, resulting in the correlations with $\sigma_t^0$ seen in Table 1.

Therefore, the relationship between soil moisture and $\sigma_t^0$ should be greatest in a bare peat environment. In this setting, there is significant seasonal variation in WTD, but limited vegetation cover to affect $\sigma_c^0$, $\sigma_m^0$, or $\sigma_d^0$.

## 1.2. Monitoring peatland water table depth using multi-sensor approaches

Optical remote sensing has also been applied to peatland observation. In this paper, Sentinel-2 is used. This is a companion platform to Sentinel-1 that is also part of the European Union's Copernicus programme. Currently, the Sentinel-2 mission is a constellation of satellites (Sentinel-2A, launched in June 2015, and Sentinel-2B, launched in March 2017), with a 5-day return period (European Space Agency, 2024a). It images in 13 spectral bands, with spatial resolutions varying from 10 m to 60 m (European Space Agency, 2024b). Bhatnagar et al. (2020) used Sentinel-2 indices to map vegetation communities at
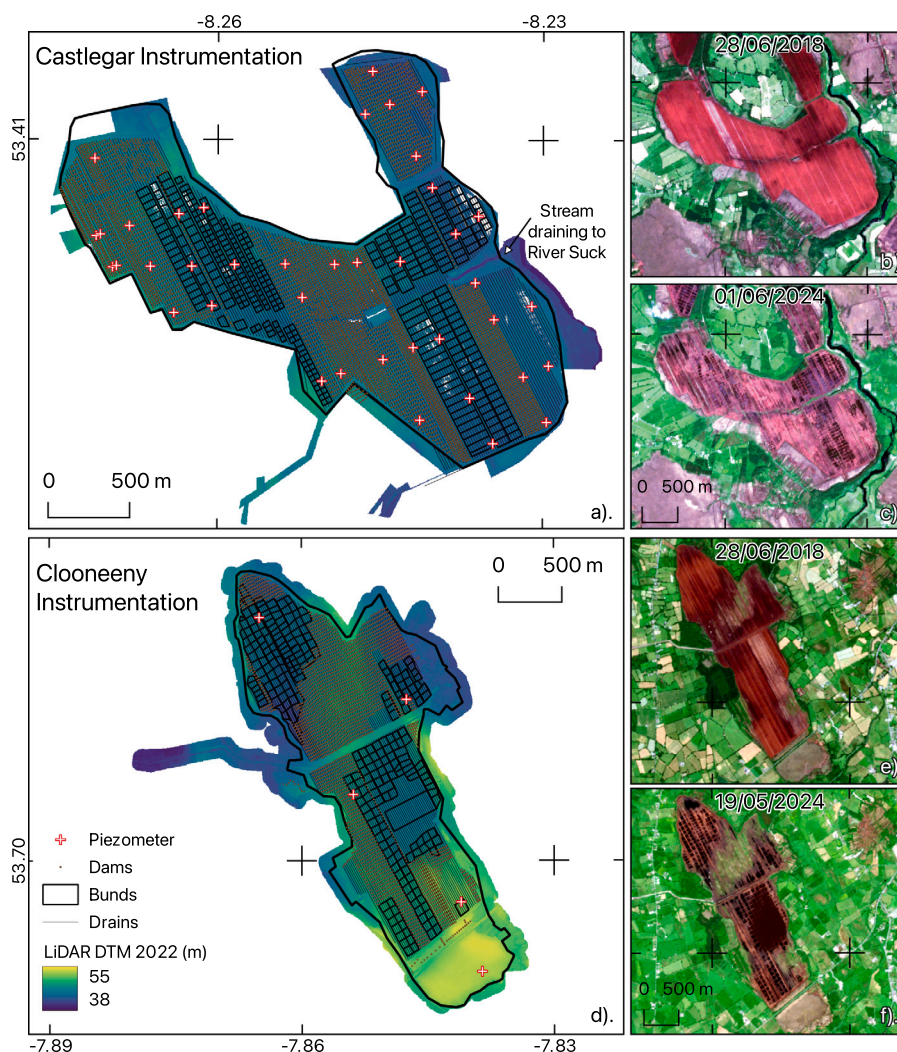
**Fig. 1.** Summary of rewetting measures implemented at Castlegar and Clooneeny bogs. (a). LiDAR digital terrain model of surface elevation at Castlegar bog. Annotated are drains, dams, bunds, piezometers, and stream location. (b). True-color Sentinel-2 image, acquired on 28/06/2018, showing Castlegar bog before rewetting strategies had been implemented. (c). True-color Sentinel-2 image, acquired on 01/06/2024, showing Castlegar bog after rewetting strategies had been implemented. (d). LiDAR Digital Terrain Model of surface elevation at Clooneeny bog. Annotated are drains, drain dams, bunds, and piezometers. This figure was made by adapting data from Bord na Móna. (e). True-color Sentinel-2 image, acquired on 28/06/2018, showing Clooneeny bog before rewetting strategies had been implemented. (f). True-color Sentinel-2 image, acquired on 19/05/2024, showing Clooneeny bog after rewetting strategies had been implemented.

multiple Irish peatlands, while Ingle et al. (2023) used high-resolution PlanetScope imagery to map vegetation and upscale $CH_4$ fluxes at Irish peatlands. Other studies have found a relationship between shortwave infrared (SWIR) imagery and WTD (Burdun et al., 2020; Räsänen et al., 2022; Isoaho et al., 2024). Multi-sensor approaches, those that combine satellite radar and optical imagery, have used machine learning models to predict WTD with good success. Räsänen et al. (2022) use a Random Forest approach with Sentinel-1, Sentinel-2, and Landsat data, to predict WTD in Finnish peatlands, with average $R^2$ of 43.1%. They studied 50 sites, each with an individual WTD monitoring station. Isoaho et al. (2024) use a similar approach, using 268 WTD measurements at six Finnish peatlands, with a model $R^2$ of 0.71 and RMSE of 0.06 m. In both these studies SWIR indices were the most important features for predicting WTD, while SAR indices were of limited importance.

Despite the limited importance of SAR, model performance was still improved when SAR data was considered in Isoaho et al. (2024). As such, SAR data are considered here. Additionally, the dense in-situ network of piezometers at the peatlands included in the current paper present a robust dataset on which to test the temporal and spatial variability of correlation between $\sigma_t^0$ and WTD, as identified by previous studies.

## 2. Materials and methods

Here, Sentinel-1 and Sentinel-2 radar and optical data were used to investigate WTD. This was done using two approaches, correlation analysis and machine learning. For correlation analysis, the data were filtered using water level limits and meteorological data (Section 2.2) before analysis was performed (Section 2.3). For the machine learning model, both SAR and optical data are prepared alongside meteorological and in-situ data (Section 2.4), before machine learning analysis performed (Section 2.5). Decision tree models (Random Forest and Gradient Boosting) are compared and validated using out-of-bag scoring and cross-validation, before making new predictions of WTD.

### 2.1. Study sites

Castlegar bog (Latitude: 53.398, Longitude: −8.249) is located in east County Galway, bordering County Roscommon (Fig. 1). This raised peatland was subjected to commercial peat extraction for >20 years by Bord na Móna (a semi-state company responsible for developing and maintaining Irish peatlands), until 2018 (Jennings O'Donovan & Partners Limited, 2021). Peat harvested from the site was used as fuel

in power stations, though as commercial harvesting here was relatively short-lived, peat depths in excess of 4 m still exist throughout much of the site (Jennings O'Donovan & Partners Limited, 2021). The majority of landcover at Castlegar is bare peat, though there are some areas of birch woodland and heather (Jennings O'Donovan & Partners Limited, 2021). The River Suck runs parallel to the site, and is connected to the peatland by a stream to the east of the site (Fig. 1). In-situ monitoring here consists of 45 piezometers, sampling at hourly intervals, with data available from 19/12/2020–02/08/2023.

Clooneeny bog (Latitude: 53.708, Longitude: −7.853) is located in County Longford, approximately 3 km west of Longford Town (Fig. 1). Industrial-scale peat harvesting was undertaken here by Bord na Móna for >30 years, from 1985–2018, and used as fuel in the Lanesborough power station (Planning and Consultants, 2022). Despite the extended timescale of harvesting, remnant peat depths typically exceed 2 m, with some areas as deep as 4 m and as shallow as 1 m (Planning and Consultants, 2022). Clooneeny bog is primarily drained by the River Fallan to its west (Planning and Consultants, 2022). Like Castlegar bog, landcover is primarily bare peat, with some areas of birch scrub, heather, and grassland Planning and Consultants (2022). In-situ monitoring here consists of six piezometers, sampling at hourly intervals, with data available from 18/12/2021–06/06/2023. Met stations at Mt. Dillon (Latitude: 53.727, Longitude: −7.981), Lecarrow (Latitude: 53.544, Longitude: −8.047), and Athenry (Latitude: 53.289, Longitude: −8.786), provide daily historical measurements of meteorological parameters, providing data indicative of on-site conditions, for both peatlands. At Clooneeny, rewetting features were not installed until August 2022, limiting the available satellite data when compared to Castlegar.

To date, rewetting strategies have consisted of drain blocking, bund installation, and *Sphagnum* inoculation at various locations throughout both Castlegar and Clooneeny (Jennings O'Donovan & Partners Limited, 2021; Planning and Consultants, 2022). These efforts have transformed the topography of both sites from their degraded bare peat state. In Fig. 1, this transformation can be seen in the darker (wetter) areas in true-colour Sentinel-2 images from 2018 and 2024, acquired pre-, and post-restoration, respectively. The recent restoration efforts (temporally overlapping with the Sentinel-1 and Sentinel-2 missions), extensive bare peat surfaces, and dense in-situ piezometer network, make Castlegar and Clooneeny bogs ideal study candidates for satellite-based remote sensing, and offer a unique opportunity to systematically investigate the relationship between radar-backscatter, optical indices, and WTD.

### 2.2. Data preprocessing for SAR–water table depth correlation analysis

To compare water level with SAR backscatter, data from 40 piezometers at Castlegar bog were used (data from 5 deep piezometers were not used), from 01-01-2021 to 31-12-2023 (Figure A.7). The relationship at Clooneeny was not considered, as there are much fewer piezometer measurements (six, Fig. 1).

#### 2.2.1. Preparation of SAR data

Sentinel-1 L1 GRD-HD files from 15-01-2021–31-12-2023 (descending) and 17-02-2021–22-12-2023 (ascending) were downloaded using the Alaska Satellite Facility Data Search Vertex (https://search.asf.alaska.edu/). The entire processing and analytical workflow conducted here are presented in Fig. 2. GRD (Ground Range Detected) data have been multi-looked and projected to ground range from SLC files. Frame 413, on path 23, was used in the descending flight direction, and frame 173 path 74 in ascending. These data were then processed with the Sentinel Applications Platform (SNAP), using the Graph workflow builder. The graph files detailing the steps taken to process these data are freely accessible (See Data and Code Availability). Once each scene had been processed, they were coregistered as a multi-temporal stack. Speckle noise is the primary source of noise in radar backscatter images

and was corrected by filtering this stack using a multi-temporal Lee Sigma speckle filter. This workflow was performed using both the VV and VH polarised bands, varying the level of multi-looking to create output stacks with pixel spacing of 30 m.

#### 2.2.2. Water level filtering

The WTD data were provided by Bord na Móna, and form a robust dataset of measurements of water level from the surface. Hourly time series of WTD for every piezometer and average site-wide WTD are presented in Figures A.7 and A.8. Prior to correlation analysis, these hourly sampled time series were resampled to daily average values. In addition, any dates where the water level is >0 m (that is, when there is surface water) were filtered. This was done as surface water acts as a specular reflector, resulting in backscatter signals that are not associated with surface scattering.

#### 2.2.3. Environmental filtering

The data were filtered using rainfall measurements from the Met Éireann Historical Data portal (https://www.met.ie/climate/available-data/historical-data). Days where total rainfall exceeded 20 mm were filtered, as were those where the soil temperature at 0.10 m depth was less than 4 °C (after Bechtold et al. (2018) and Lees et al. (2021)). Excessive rainfall or freezing may alter soil backscatter characteristics, and result in a spurious relationship between $\sigma_t^0$ and WTD. Historical meteorological data from the Mt. Dillon weather station (Lat.: 53.727, Lon.: −7.981) were used to filter by ground temperature, and from the Lecarrow weather station (Lat.: 53.544, Lon.: −8.047) to filter by rainfall — these were selected as they are the closest stations to the peatland that record their respective parameters. Though vegetative corrections have been shown to significantly affect the correlation coefficient between $\sigma_t^0$ and WTD (Bechtold et al., 2018; Lees et al., 2021; Räsänen et al., 2022; Lees et al., 2021), such corrections are not applied to the data here as both peatlands in this study are in a post-industrial state, and are dominated by bare peat surfaces.

### 2.3. SAR–water table depth correlation analysis

For each piezometer and its corresponding pixel, the Pearsons correlation coefficient ($R$) between the water level data and SAR backscatter intensity was calculated, in both polarisations and track directions. This calculation was then performed at each piezometer both spatially and temporally. Spatial correlation analysis was also performed using selected optical indices, from the dataset described below.

### 2.4. Data preprocessing for machine learning

Machine learning algorithms were also used to effectively model WTD. Here, SAR data were used alongside optical satellite data, in-situ measurements, and meteorological data (Fig. 2).

#### 2.4.1. Preparation of satellite data

Both Sentinel-1 and Sentinel-2 provide year-round, regular coverage of the study sites. Here, data with zero-day separation were selected (e.g. both satellites imaged the target peatlands on the same day). As a result, cloud cover in Sentinel-2 imagery is the primary control on the satellite data included here. To identify suitable dates, every Sentinel-2 acquisition across the study period was filtered (January 2021–June 2023 at Castlegar, and August 2022–June 2023 at Clooneeny) so that cloud cover across the entire scene was < 50% (on the Copernicus Browser: https://browser.dataspace.copernicus.eu/). The study period is defined by when there was available piezometer data, following rewetting. Dates where the study sites were partially or wholly visible were identified and compared with Sentinel-1 acquisitions to identify same-day data for both satellites. These dates were downloaded and processed before further analysis. The used acquisition dates are presented in Table A.2.
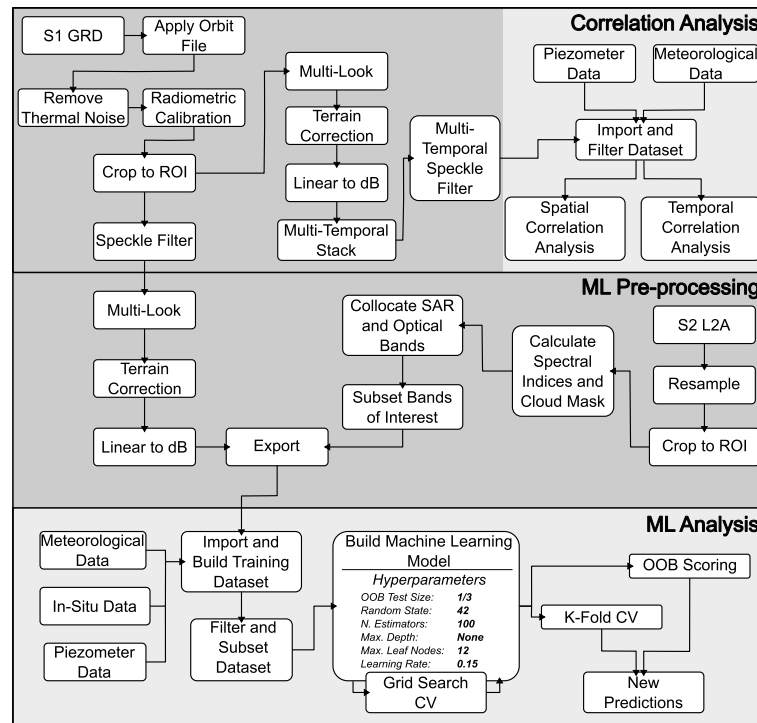
**Fig. 2.** Schematic describing the processing and analytical workflow for both correlation and machine learning analysis. Dark grey represents elements of the workflow that were conducted in ESA's SNAP software (e.g. data processing), while light grey represents elements that were carried out in Python (e.g. data analysis). The in-figure hyperparameters refer to those used in Gradient Boosting.

The same workflow as Section 2.2.1 was followed (Fig. 2), with key differences. As individual dates were processed, coregistered multi-temporal stacks were not created. Therefore, multi-temporal speckle filtering could not be performed, and instead spatial filtering was used prior to multi-looking. The SAR data were multi-looked to 30 m pixel spacing, and exported as geotiff products. This workflow was repeated for both VV and VH polarisations. Vegetative corrections were not applied to these data either.

Sentinel-2 L2a bottom-of-atmosphere products were downloaded from the Copernicus Dataspace Browser (https://browser.dataspace.copernicus.eu/), and processed using SNAP. L2a products have been atmospherically corrected, are a "Bottom-Of-Atmosphere" reflectance product, and include Scene Classification Layers. These layers classify sources of noise in the scene, which is reduced by masking areas classified as cloud shadow, snow and ice, as well as cirrus clouds, and areas of medium and high cloud probability. These were again processed using the graph workflow, with graph files detailing the processing steps available in the Data and Code Availability section. To ensure seamless data fusion between Sentinel-1 and Sentinel-2, these data were resampled to 30 m pixel resolution (matching that of Sentinel-1), before being collocated, using the collocate function in the Raster Toolbox in SNAP. Here, each band from both platforms are aligned to a common geographical raster, to ensure consistent pixel indices during further analyses. Following this, the subset tool was used, this time to extract the relevant bands. The final product contained the following bands, ordered as: VV, NDVI, NDWI, STR, SAVI, CloudMask, TCG, TCW, Blue, Green, Red, NIR, SWIR1, SWIR2, VH, and was exported in BigTIFF format (Non-abbreviated names are listed in Table A.3). In addition to the machine learning approach described below, correlation analysis was also performed between selected optical indices (STR, SWIR1, SWIR2, NDWI, NDVI and Blue) and WTD at Castlegar, using the optical imagery contained in this dataset (Table A.2, Figure A.9).

As optical indices were considered in the machine learning model, environmental filtering (ground temperature, rainfall) was not carried out on this dataset (e.g. Bechtold et al. (2018) and Lees et al. (2021)),

as such indices are not affected by specular reflection. Instead, meteorological data were used as predictor variables (Section 2.4.3), and days where WTD is >0 m are considered. In order to account for the different acquisition times of Sentinel-1 and Sentinel-2, the average WTD for each day was considered as the target variable.

### 2.4.2. Ground data

In-situ data were added to the datasets to add further constraints to the model, in order to investigate the influence of re-wetting features (Fig. 2). These were: distance from point to nearest bund, distance from point to nearest peat dam, and peat depth. For the training dataset, each of these were calculated from the location of each piezometer, while for the new predictions dataset, distances and depths were calculated for every point across the entire peatland. Peat depths were provided by Bord na Móna, while distances were calculated in QGIS with the following workflow (visualised in Figure A.10): each data point was expressed as a point shapefile, either from a CSV of piezometer locations, or with the "Raster Pixels to Points" tool, using 30 m SAR rasters. The outline of the bunds were expressed as point layers, every 0.5 m, using the "Points Along Geometry" tool. The closest peat dam, closest bund edge to each piezometer, and testing point were calculated using the "Distance to Nearest Hub" tool. The depth of peat at each relevant point was calculated from the peat depth layer, using the "Sample Raster Values" tool. A final CSV file was exported containing latitude and longitude data for each point, the underlying depth of peat, the distance to the nearest bund, and distance to the nearest dam.

### 2.4.3. Meteorological data

To add further model constraints meteorological variables were also considered, namely the average maximum air temperature, and soil temperature on the day of satellite acquisition. These data were selected as they were freely accessible and available historically, thereby allowing the testing of the relationship between WTD and meteorological variables. These were recorded at Athenry, and Mt Dillon weather stations, respectively, and again downloaded at daily resolution from the Met Éireann Historical Data portal (https://www.met.ie/climate/available-data/historical-data).
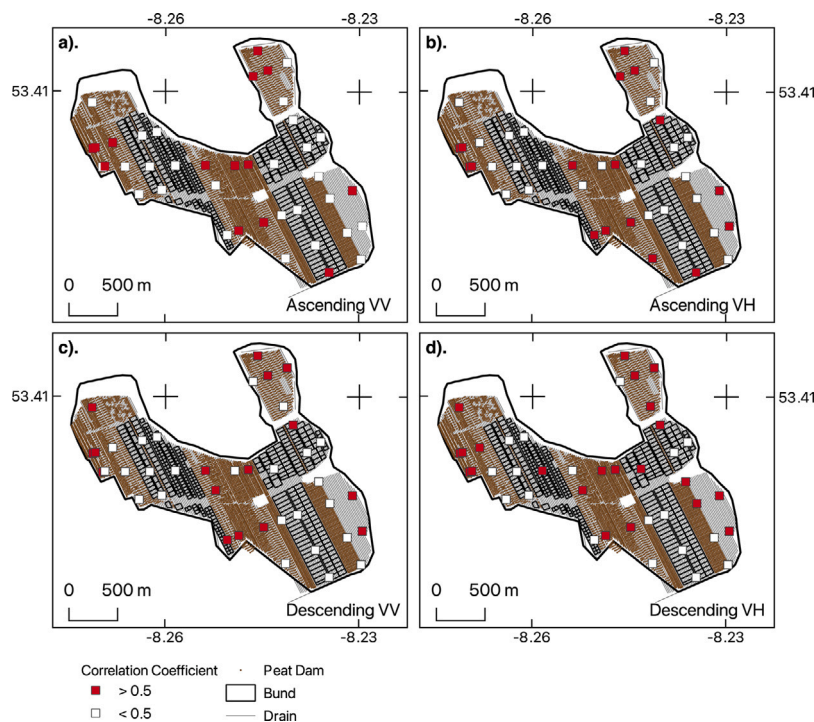
**Fig. 3.** Spatial distribution of correlation at piezometers between $\sigma_t^0$ and WTD at Castlegar, in both VV and VH polarisations in ascending and descending track directions. (a). Absolute correlation coefficients of >0.5 between WTD and $\sigma_t^0$, in ascending VV polarisation. (b). Absolute correlation coefficients of >0.5 between WTD and $\sigma_t^0$, in ascending VH polarisation. (c). Absolute correlation coefficients of >0.5 between WTD and $\sigma_t^0$, in descending VV polarisation. (d). Absolute correlation coefficients of >0.5 between WTD and $\sigma_t^0$, in descending VH polarisation. In all sub-plots, the extent of Castlegar bog is outlined in black, while installed drains, the location of drain dams and bunds are annotated. This figure was made by adapting data from Bord na Móna.

### 2.5. Machine learning predictions of water table depth

Both a Random Forest model (aggregate of multiple decision tree regressions (e.g. a "Forest")), and a Gradient Boosting Model (uses weak learners (short decision trees), and a differentiable loss function to predict the target variable) were tested (e.g. after the Random Forest modelling of Räsänen et al. (2022) and Isoaho et al. (2024)). All modelling was performed using the scikit-learn (sklearn) module in Python (Pedregosa et al., 2011).

The SNAP products were imported for each date, and the relevant variable (e.g. NDVI) was selected for the index at the geographic co-ordinate at each piezometer. Cloud Masks, calculated in Section 2.4.1, were then applied, to remove data that had been obscured by clouds. At each geographic index (piezometer location) the peat depth, distance to bund, and distance to peat dam was appended, as was the meteorological data for each date (Section 2.4.3). This was carried out using data from both Castlegar and Clooneeny bogs. The final formatted product was a Pandas DataFrame, containing 20 columns (though this number decreased with later filtering during feature importance testing), of which WTD was the target variable. This DataFrame contained 620 points, on which the model was trained and tested.

#### 2.5.1. Model validation

Model performance was evaluated using both out-of-bag testing and k-fold cross-validation (Fig. 2). In out-of-bag scoring, a fraction of the dataset ($\frac{1}{3}$ in this case) is withheld when training the model, and then used to test model performance by comparing predicted values to their known values. The data are shuffled prior to splitting, meaning that values are randomly sampled spatially and temporally. In k-fold cross validation, the data are first shuffled, before being subset into a number of equal size samples (given by $k$). Each subset is then withheld from the training dataset, and used to evaluate the performance of the model, trained on the rest of the data. This was performed $k$ times, to evaluate how the model performs across the entire dataset. The

model feature importance (how important is each predictor variable in predicting the target variable) was also determined, as a way to determine potential noise variables. These were determined with the "feature_importances_" attribute in sklearn, where importance is determined by the average reduction in mean square error by each feature as well as by using SHAP values (SHapely Additive exPlanations: measures of how each feature contributes to a model's prediction). The model was ran repeatedly, and the poorest performing variable systematically removed, until there was no performance improvement in either $R^2$ or RMSE. An example of the final filtered variables are presented in Table A.4. Though these features represent best model performance, models were also evaluated with no SAR data, no ancillary variables, and individual ground-based variables (Figures A.11, A.12, and A.13). Hyperparameter testing was performed to tune the model using Grid Search Cross Validation (Table A.5). This resulted in the following settings in the Gradient Boosting model: 100 iterations, with a maximum of 12 leaf nodes in each decision tree, a learning rate of 0.15. Here, and when splitting the data during out-of-bag validation, the "random_state" value (random generator seed value) was set to 42 (to ensure reproducibility between model runs).

#### 2.5.2. New predictions of water table depth

Given the good model performance in cross validation (Table A.6), the entire dataset was used to train the Gradient Boosting model, which was then used to make predictions of WTD across entire peatlands. Four dates were selected for predictions at each peatland, two from the growing season and two during winter. At Castlegar these were 25-04-2021, 29-06-2021, 21-11-2021, 16-11-2022, while at Clooneeny these were 29-06-2021, 28-08-2021, 21-11-2021, and 16-11-2022. The new predictions dataset was prepared in exactly the same way as the training dataset. However, for the date of interest, predictor variables are determined at every pixel across the peatland (e.g. with 30 m spacing), instead of just at the piezometer coordinates, and there was no column containing target (WTD) values. The trained model was then used on this dataset to predict WTD across the entire peatland.
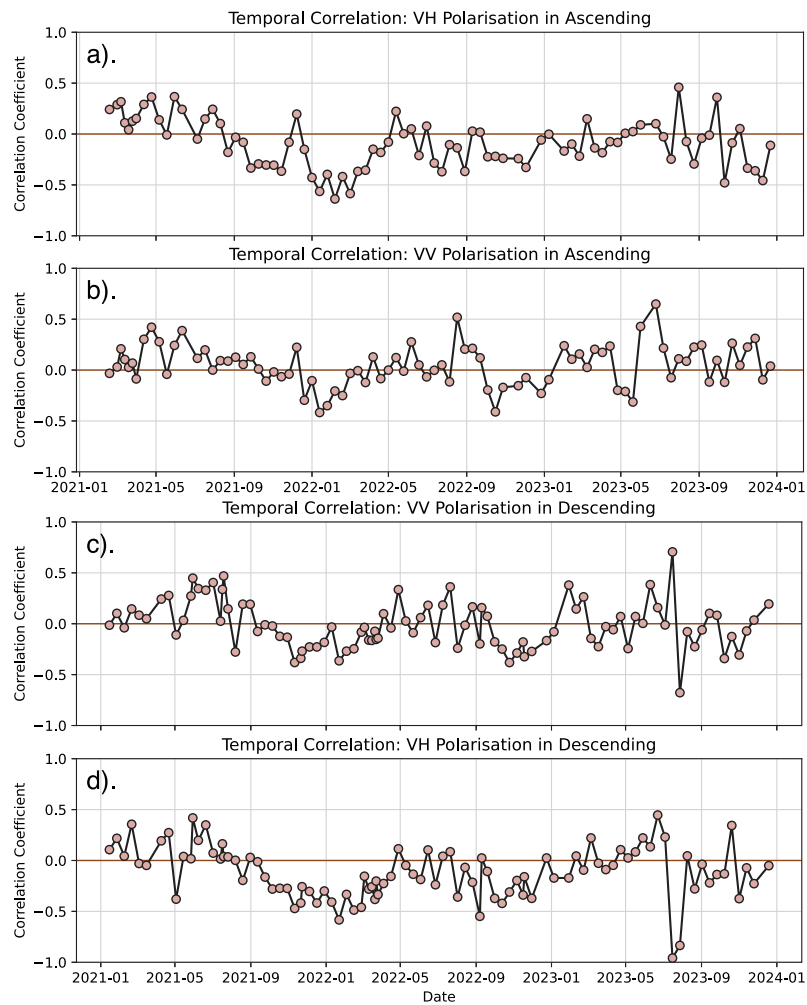
**Fig. 4.** Temporal correlation between $\sigma_t^0$ and WTD at Castlegar, in both VV and VH polarisations in ascending and descending track directions. (a). Correlation coefficients between WTD and $\sigma_t^0$, in ascending VH polarisation. (b). Correlation coefficients between WTD and $\sigma_t^0$, in ascending VV polarisation. (c). Correlation coefficients between WTD and $\sigma_t^0$, in descending VV polarisation. (d). Correlation coefficients between WTD and $\sigma_t^0$, in descending VH polarisation.

## 3. Results

### 3.1. Correlation between water table depth and radar backscatter at castlegar

In both polarisations and track directions, there are a range of correlation coefficient values between $\sigma_t^0$ and WTD depth at each filtered piezometer (Fig. 3). Spatially, the VH polarisation in the descending track has minimum values of $-0.13$ (a weak negative correlation) and maximum values of $0.75$ (moderate–strong positive correlation), with minimum values of $-0.19$ and maximum values of $0.78$ in VV polarisation. Similarly in ascending, the VH polarisation has minimum values of $-0.12$ and maximum values of $0.72$, with minimum values of $-0.3$ and maximum values of $0.76$ in VV polarisation. In both track directions, VH polarisation is more strongly correlated with WTD than VV, with VH correlation coefficients of $>|\,0.5\,|$ at 55% and 43% of piezometers in descending and ascending tracks, respectively. This decreases to at 40% and 35% for piezometers in VV polarisation in descending and ascending tracks, respectively.

In both polarisations, areas where correlation between $\sigma_t^0$ and WTD is consistently well correlated ($>|\,0.5\,|$) are identified. The land surface at each of these locations is characterised by flat, bare peat surfaces, with minimal topographic changes. Under these conditions, the relationship between WTD and $\sigma_t^0$ is strongest, as there is no vegetation and consistent surface scattering properties. In Fig. 3 the correlation

between $\sigma_t^0$ and WTD at each piezometer, overlaid on restoration structures at Castlegar, are presented. From this, the following characteristics can be identified: strongly correlated piezometers are generally located in the open peatland, away from bunds. The majority of poorly correlated piezometers are located in, or adjacent to bunds. This is consistent between both polarisations, in both track directions. In the southeastern sector of the peatland, there is a series of four piezometers that are generally poorly correlated, that occur along the boundary between dammed peatland and undammed peatland. This result led to the inclusion of rewetting parameters (e.g. distance to bund) in the machine learning model.

Temporal correlation analaysis (e.g. the correlation coefficients between $\sigma_t^0$ and WTD are calculated through time rather than through space) provides a better insight into how the relationship between $\sigma_t^0$ and WTD changes through time (Fig. 4). For each track direction and polarisation, there is a seasonal alteration between more positive and more negative correlation. All results show more negative site-wide correlation in during the winter months (January, Fig. 4), and more positive correlations during the summer months (June–July, Fig. 4).

Correlation analysis of optical indices (Figure A.9) shows correlation coefficients of $>|\,0.5\,|$ at most tested piezometers. The direction of relationship changes between indices, with STR, NDWI, and NDVI are positively correlated, and SWIR1, SWIR2, and Blue are negatively correlated. This correlation analsysis may be further imporved with the consideration of more dates, as the tested optical dataset (24 dates)
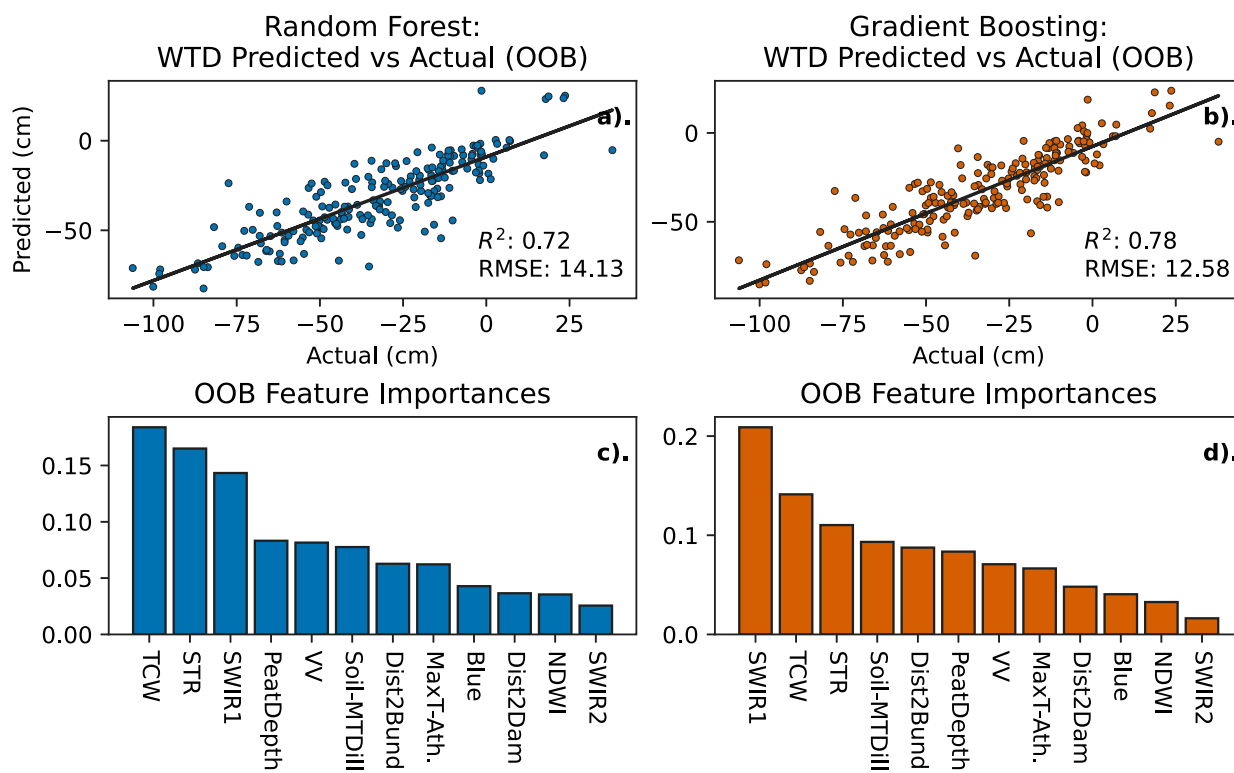
**Fig. 5.** Model validation and feature importance comparison between Random Forest and Gradient Boosting models, using data from both Castlegar and Clooneeny. The model scores are presented in Table A.6. (a). Predicted vs. actual WTD values for out-of-bag Random Forest validation. A linear regression fit is indicated by the black line. (b). Predicted vs. actual WTD values for out-of-bag Gradient Boosting validation. A linear regression fit is indicated by the black line. (c). Feature importances for out-of-bag Random Forest validation. (d). Feature importances for out-of-bag Gradient Boosting validation.

was much smaller than the tested SAR datasets (85 and 97 dates in ascending and descending tracks, respectively).

### 3.2. Model feature importance

Results of model validation are presented in Fig. 5, with out-of-bag testing showing Gradient Boosting to be an improved predictor to Random Forest (Table A.6), with out-of-bag $R^2$ values of 0.78 and 0.72, respectively. Though each model performs differently, there are some key similarities: the most significant features (top two or three in Fig. 5) in every validation are optical indices relating to SWIR, and tassled cap wetness. SAR indices have consistently poor feature importance. VV polarised backscatter is consistently a moderately performing feature. VH polarised backscatter is removed from the final model run as it is a borderline noise index: both $R^2$ and RMSE scores improve when it is removed from the model. In-situ data concerning re-wetting structures and meteorological data are moderately important features: they are unlikely to predict WTD by themselves, but improve model performance when included with satellite data. Model features were further interrogated using SHAP values. These again showed that shortwave indices contribute the most to the model output, followed by in-situ data, other optical indices, and SAR data (Figure A.14). Interpreting these values (Figure A.15 and Figure A.16) enabled deeper analysis of feature importance. For both STR and TCW, low values correspond to a deeper WTD, while for other shortwave indices (e.g. SWIR1 and SWIR2), low values correspond to a higher WTD. These values also illustrate the impact of meteorological data on the model performance. For example, days of higher soil temperature, correspond to a deepening in WTD, as shown in Figure A.15 and Figure A.16. This analysis shows features that have a synergistic relationship (e.g. low values of STR and peat depth correspond to deeper WTD), while features such as soil temperature and TCW have an antagonistic relationship.

When SAR variables were removed from the gradient boosting model, out-of-bag $R^2$ was 0.77 and RMSE was 12.74 (Figure A.11). When all non-satellite variables were removed from the gradient boosting model, out-of-bag $R^2$ was 0.51 and RMSE was 18.53 (Figure A.12). When distance to bund was the sole in-situ measurement, out-of-bag $R^2$ was 0.7 and RMSE was 14.54 (Figure A.13). In Figure A.17, new predictions of WTD at Ballaghurt bog (53.321, −7.875) were made with no in-situ variables, though with greatly diminished model performance ($R^2 < 0.6$).

### 3.3. Predicting water table depth

Predicted WTDs from the Gradient Boosting model are presented as spatial maps in Fig. 6. Predictions of estimated minimum, median, mean, and maximum WTD are also presented in Table A.7. The lack of data from 2021 at Clooneeny limited the available dates at Clooneeny, resulting in partial predictions in Fig. 6, as dates with some cloud cover are predicted. The WTD at Castlegar is consistently shallower than that at Clooneeny. On 16-11-2022 the WTD at Castlegar is >0.1 m shallower (Table A.7). The WTD at both peatlands was much shallower in the winter than during the growing season. At both peatlands both predictions of growing season WTD were over twice as deep as the predictions of winter WTD. At both sites, areas where bunds have been established are visible in predictions, and typically have shallower WTDs (Fig. 6).

### 3.4. Prediction intervals

Uncertainty is quantified by calculating 90% prediction intervals, using the 5% and 95% quantiles – e.g. the range within which the prediction is expected to fall, 90% of the time. These intervals are presented in Figure A.18, and have an average range of approximately
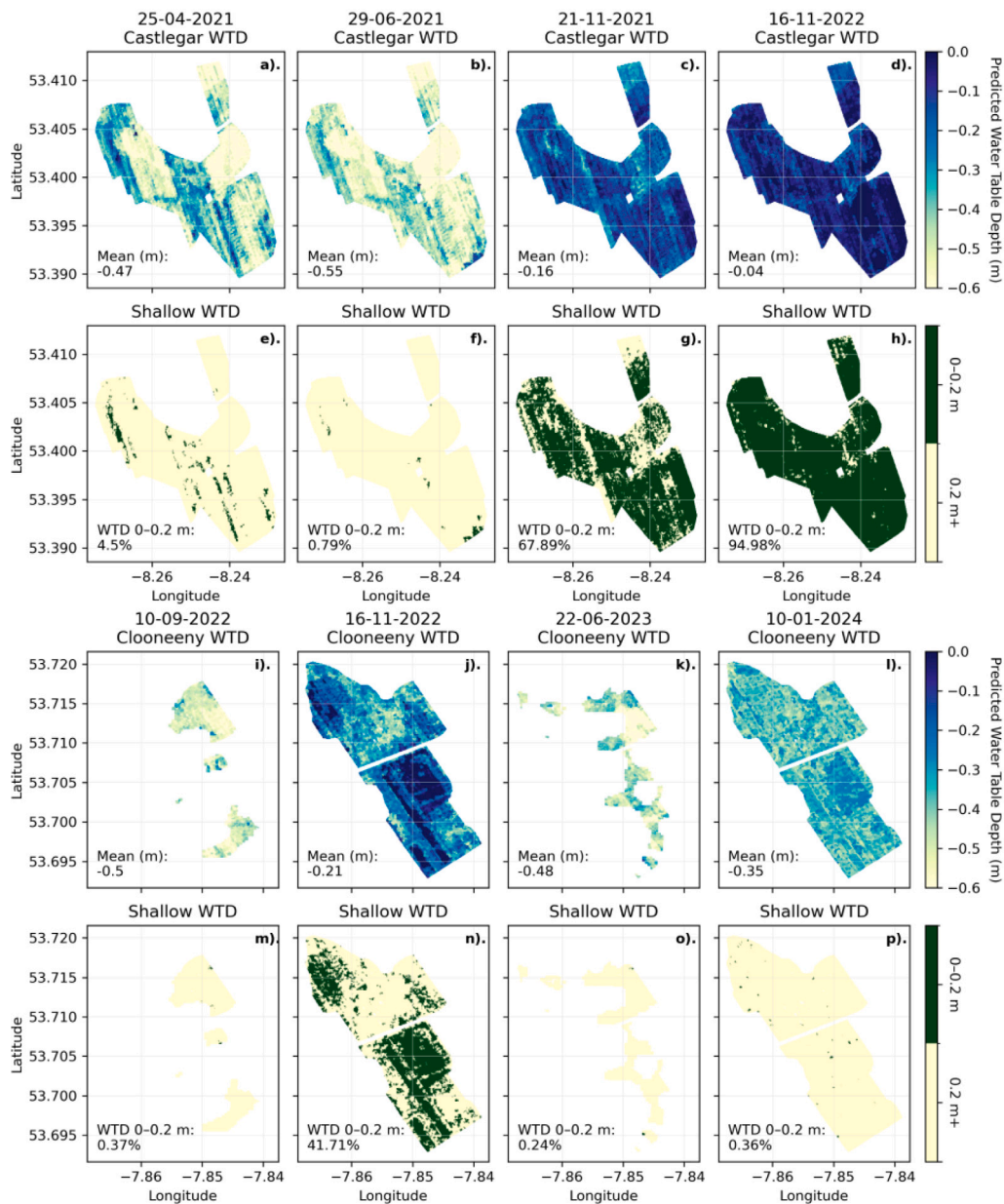
**Fig. 6.** Maps of predicted water table depth at Castlegar and Clooneeny bogs, annotated with the average predicted water table depth, and percentage of shallow water table depth. Here, shallow water table depth refers to the optimal range for rewetting of shallower than −0.2 m from the surface. Predicted water table depth at Castlegar on (a). 29-06-2021. (b). 21-11-2021. (c). 16-11-2022. (d). 10-01-2024. Fraction of water table depth deeper that −0.2 m at Castlegar, on (e). 29-06-2021. (f). 21-11-2021. (g). 16-11-2022. (h). 10-01-2024. Predicted water table depth at Clooneeny, on (i). 29-06-2021. (j). 21-11-2021. (k). 16-11-2022. (l). 10-01-2024. Fraction of water table depth deeper than −0.2 m at Clooneeny, on (m). 29-06-2021. (n). 21-11-2021. (o). 16-11-2022. (p). 10-01-2024. White areas on 10-09-2022, and 22-06-2023 denote areas where clouds have been masked from the Sentinel-2 imagery.

0.4 m. The range between the 25% and 75% prediction interval quartiles is approximately 0.1 m. These predictions show (Figure A.18), that even when uncertainty is accounted for, the average growing season WTD is less than the ideal 0.2 m below the surface required for effective peatland management.

## 4. Discussion

### 4.1. Controls on correlation between WTD and radar backscatter

The strength of the relationship between WTD and $\sigma_t^0$ varies spatially and temporally (Figs. 3 and 4), and there is no clear way of using $\sigma_t^0$ alone as a predictive tool. Like the studies presented in Table 1 (e.g. Kasischke et al. (2003) and Hrysiewicz et al. (2023)), Fig. 3

shows a range of correlation strengths, from which the following can be observed: the strongest correlation between WTD and $\sigma_t^0$ occurs when the studied point is located in open peatland, away from rewetting structures such as bunds. Here, topographic changes introduced by bunds may be sufficient to decrease the correlation between $\sigma_t^0$ and WTD. In these locations, there are two surfaces that radar waves are scattering off (top of bund and trough of bund), each a separate distance to the water table. In some locations piezometers are consistently poorly correlated, despite being in open, flat peatland. In the absence of any adjacent rewetting structures to this poor correlation, it is possible that local topography or vegetation is impacting the relationship between WTD and $\sigma_t^0$. In these locations, vegetative corrections may increase the strength of the relationship (Wagner et al., 1999; Lees et al., 2021), though the degree of vegetative cover should be first quantified before performing such corrections. The seasonal alteration

between positive and negative correlation (Fig. 4) shows that SAR backscatter may be used to indicate seasonal shallowing and deepening of WTD, though again, with limited utility as a predictive tool.

### 4.2. Seasonal water table depth at castlegar and clooneeny

As discussed in Section 1, peatland WTD must be shallower than −0.2 m (and ideally between −0.05 to −0.13 m) to promote optimal restoration conditions (Regan et al., 2020; Evans et al., 2021). The site-wide WTD at both peatlands predicted here varies significantly throughout the year (Fig. 6), with the shallowest WTD occurring during the winter months, and the deepest during the spring and summer months. This variation in WTD suggests that optimal conditions only exist for part of the year; during winter much of the peatland may have a net negative GHG balance (e.g. act as a sink), and have suitable conditions for *Sphagnum* growth (three of four winter-time predictions of average WTD at Castlegar and Clooneeny are < 0.2 m below the surface) (Regan et al., 2020; Evans et al., 2021). However, vegetation growth is limited there during the winter months, meaning that despite suitable WTDs, $CO_2$ assimilation is most likely negligible. During the summer months, every predicted WTD is deeper than the optimal range (Fig. 6), suggesting that the peatlands are acting as both a net source of GHG (Evans et al., 2021), and are simultaneously not sequestering $CO_2$. However, due to data availability, the majority of dates where WTD was predicted are from 2021, when Sentinel-1A and Sentinel-1B were still in constellation. The average WTD at Castlegar has shallowed since then (Figure A.7), suggesting that rewetting conditions may have improved since these dates.

### 4.3. Management implications for peatland rewetting

This study demonstrates the usefulness of multi-sensor remote sensing in modelling peatland WTD, and indicates that satellite remote sensing may be a powerful tool in the management of peatland restoration (Monteverde et al., 2022). The ability to predict WTD site-wide over several square kilometres may greatly complement in-situ instrumentation, allowing for evaluation of the restoration of entire peatlands (Isoaho et al., 2024), rather than of instrumented localities (Asmuß et al., 2019). Additionally, the data, software, and code used here are wholly open-source and free to access, and require no specialist computational facilities (Data and Code Availability). The research presented here was conducted using an Apple Macbook Air with an M2 processor, and 8 GB of RAM. The Sentinel-1 and Sentinel-2 files were up to 2 GB in size, and the final processed stacks output from SNAP were approximately 20 MB. Maximum memory usage during model training was approximately 800 MB, and approximately 900 MB when making new predictions. Given the low computational cost, this approach is scalable to include greater spatial coverage, more complex models, or higher resolution data. As such, this approach may be freely implemented into ongoing management plans, allowing for continuous modelling of WTD.

It should be borne in mind that the dates predicted here required a cloud-free Sentinel-2 acquisition in order to be modelled. Cloud-free weather is typically associated with low-levels of precipitation, and accordingly, a potential lowering of WTD (Bechtold et al., 2018). A key inhibitor to the model performance is the requirement for same-day acquisitions of Sentinel-1 and cloud-free Sentinel-2. However, as shown in Fig. 5, SAR backscatter intensity does not significantly improve model performance. Additionally, as shown in Fig. 6, the majority of predicted dates are from before 2022. During this time, both Sentinel-1A and Sentinel-1B were in constellation, allowing for more frequent same-day Sentinel-1 and Sentinel-2 acquisitions. The comparatively limited data from the single satellite Sentinel-1 mission (as was the case during this study) greatly inhibits the potential of multi-sensor SAR and optical analyses. The importance of optical indices as model features here, good model performance when SAR is not included, and previous

studies (Räsänen et al., 2022; Isoaho et al., 2024), suggest that future models may benefit by the omission of Sentinel-1 data. This would greatly increase the amount of data considering in the modelling, by allowing dates where there has been a cloud-free optical acquisition to be included without the added constraint of a concurrent SAR overpass. The larger dataset may allow for more complex modelling to be performed. Deep learning techniques such as Convolutional or Recurrent Neural Networks may allow for even more accurate predictions of WTD. In the context of the management of peatland restoration, such a model would allow for site-wide evaluation of WTD, on any day with a cloud-free optical overpass.

Both peatlands modelled here are at similar stages of rewetting, consisting of extensive bare peat surfaces, peat dams, and peat bunds. There are numerous peatlands at such a stage where this model has potential to accurately predict WTD. However, for more general application, variables relating to rewetting structures and peat depth should not be considered as rewetting strategies vary site-to-site, and may not involve peat bunds or dams. In Figure A.17, we make new predictions of WTD at Ballaghurt bog, in the Irish midlands, without considering in-situ data. Though model performance is greatly diminished, this showcases the model potential in considering site-wide WTD at a much larger scale. Additionally, at rewetted peatlands that have successfully promoted vegetation growth, optical indices such as NDVI and EVI may be more significant features (given that they provide information about vegetation cover, e.g. Bhatnagar et al. (2020)). As such, a model based on optical indices, that considers the degree of vegetation at a peatland may have the best potential for general applicability and prediction of WTD. This would allow for continuous modelling throughout the progression of the rewetting process, allowing for changes in peatland WTD to be characterised, from early stage rewetting, to a fully restored peatland.

## 5. Conclusions

In this paper, multi-sensor remote sensing data and in-situ data have been used to make predictions of WTD in degraded, bare peat peatlands. Additionally, the relationship between WTD and radar backscatter intensity has been systematically tested. Clear spatial controls on this relationship have been identified, finding that it is highly sensitive to changes in surfaces scattering properties — changes in topography or surface scattering properties may decouple this relationship. Predicted WTD at both Castlegar and Clooneeny bogs show that, typically, the water table is deeper than 0.2 m below the surface. Under current conditions, restoration from this degraded, bare peat environment, to "natural" conditions is unlikely, until site-wide WTD can be maintained at shallower levels. This study has presented methodology whereby WTD may be predicted at degraded peatlands, allowing for updated measurements under certain conditions. Going forward, this approach may be applied on a larger scale, and used to predict WTDs more generally at peatlands, in order to inform restoration management strategy. This has implications nationally, in Ireland, but also internationally, as industrialised peatlands transition from a degraded status, to restored.

## CRediT authorship contribution statement

**Eoin Reddin:** Writing – original draft, Software, Methodology, Investigation, Formal analysis, Data curation, Conceptualization. **Jennifer Hanafin:** Writing – review & editing, Supervision, Methodology. **Mingming Tong:** Writing – review & editing, Supervision. **Laurence Gill:** Writing – review & editing, Supervision, Conceptualization. **Mark G. Healy:** Writing – review & editing, Supervision, Funding acquisition, Conceptualization.

## Data and code availability

The python code used to perform this modelling, as well as the trained models (as .pkl files) are freely available at https://github.com/ered22/Multi_Sensor_GB.

## Declaration of competing interest

The authors declare that they have no known competing financial interests or personal relationships that could have appeared to influence the work reported in this paper.

## Acknowledgements

## Appendix A. Supplementary data

Supplementary material related to this article can be found online at https://doi.org/10.1016/j.srs.2025.100238.

## Data availability

The python code used to perform this modelling, as well as the trained models (as .pkl files) are freely available at https://github.com/ered22/Multi_Sensor_GB.

## References

Aitova, E., Morley, T., Wilson, D., Renou-Wilson, F., 2022. A review of greenhouse gas emissions and removals from Irish peatlands. Mires Peat 29 (04), 1–17. http://dx.doi.org/10.19189/MaP.2022.SNPG.StA.2414.

Asmuß, T., Bechtold, M., Tiemeyer, B., 2019. On the potential of sentinel-1 for high resolution monitoring of water table dynamics in grasslands on organic soils. Remote. Sens. 11 (14), 1659. http://dx.doi.org/10.3390/rs11141659, URL: https://www.mdpi.com/2072-4292/11/14/1659.

Bechtold, M., Schlaffer, S., Tiemeyer, B., De Lannoy, G., 2018. Inferring water table depth dynamics from ENVISAT-ASAR C-Band backscatter over a range of peatlands from Deeply-Drained to natural conditions. Remote. Sens. 10 (4), 536. http://dx.doi.org/10.3390/rs10040536, URL: http://www.mdpi.com/2072-4292/10/4/536.

Bhatnagar, S., Gill, L., Regan, S., Naughton, O., Johnston, P., Waldren, S., Ghosh, B., 2020. Mapping vegetation communities inside wetlands using sentinel-2 imagery in Ireland. Int. J. Appl. Earth Obs. Geoinf. 88, 102083. http://dx.doi.org/10.1016/j.jag.2020.102083, URL: https://linkinghub.elsevier.com/retrieve/pii/S0303243419308359.

Burdun, I., Bechtold, M., Sagris, V., Lohila, A., Humphreys, E., Desai, A.R., Nilsson, M.B., De Lannoy, G., Mander, 2020. Satellite determination of peatland water table temporal dynamics by localizing representative pixels of a SWIR-based moisture index. Remote. Sens. 12 (18), 2936. http://dx.doi.org/10.3390/rs12182936, URL: https://www.mdpi.com/2072-4292/12/18/2936.

European Space Agency, 2024a. Sentinel-2 colour vision for copernicus. URL: www.esa.int/Applications/Observing_the_Earth/Copernicus/Sentinel-2.

European Space Agency, 2024b. Sentinel-2 spatial resolution. URL: sentinel.esa.int/en/web/sentinel/user-guides/sentinel-2-msi/resolutions/spatial.

Evans, C.D., Peacock, M., Baird, A.J., Artz, R.R.E., Burden, A., Callaghan, N., Chapman, P.J., Cooper, H.M., Coyle, M., Craig, E., Cumming, A., Dixon, S., Gauci, V., Grayson, R.P., Helfter, C., Heppell, C.M., Holden, J., Jones, D.L., Kaduk, J., Levy, P., Matthews, R., McNamara, N.P., Misselbrook, T., Oakley, S., Page, S.E., Rayment, M., Ridley, L.M., Stanley, K.M., Williamson, J.L., Worrall, F., Morrison, R., 2021. Overriding water table control on managed peatland greenhouse gas emissions. Nature 593 (7860), 548–552. http://dx.doi.org/10.1038/s41586-021-03523-1, URL: https://www.nature.com/articles/s41586-021-03523-1.

Hrysiewicz, A., Holohan, E.P., Donohue, S., Cushnan, H., 2023. SAR and InSAR data linked to soil moisture changes on a temperate raised peatland subjected to a wildfire. Remote Sens. Environ. 291, 113516. http://dx.doi.org/10.1016/j.rse.2023.113516, URL: https://linkinghub.elsevier.com/retrieve/pii/S0034425723000676.

Hrysiewicz, A., Williamson, J., Evans, C.D., Jovani-Sancho, A.J., Callaghan, N., Lyons, J., White, J., Kowalska, J., Menichino, N., Holohan, E.P., 2024. Estimation and validation of InSAR-derived surface displacements at temperate raised peatlands. Remote Sens. Environ. 311, 114232. http://dx.doi.org/10.1016/j.rse.2024.114232, URL: https://linkinghub.elsevier.com/retrieve/pii/S0034425724002505.

Ingle, R., Habib, W., Connolly, J., McCorry, M., Barry, S., Saunders, M., 2023. Upscaling methane fluxes from peatlands across a drainage gradient in Ireland using PlanetScope imagery and machine learning tools. Sci. Rep. 13 (1), 11997. http://dx.doi.org/10.1038/s41598-023-38470-6, URL: https://www.nature.com/articles/s41598-023-38470-6.

Isoaho, A., Ikkala, L., Päkkilä, L., Marttila, H., Kareksela, S., Räsänen, A., 2024. Multi-sensor satellite imagery reveals spatiotemporal changes in peatland water table after restoration. Remote Sens. Environ. 306, 114144. http://dx.doi.org/10.1016/j.rse.2024.114144, URL: https://linkinghub.elsevier.com/retrieve/pii/S003442572400155X.

Jennings O'Donovan & Partners Limited, 2021. Cutaway Bog Decommissioning and Rehabilitation Plan. Natural Impact Statement 6367, Bord Na Móna, Sligo, p. 286, URL: https://irishriverproject.com/wp-content/uploads/2022/02/castlegar-bog-nis.pdf.

Kasischke, E.S., Bourgeau-Chavez, L.L., Rober, A.R., Wyatt, K.H., Waddington, J.M., Turetsky, M.R., 2009. Effects of soil moisture and water depth on ERS SAR backscatter measurements from an Alaskan wetland complex. Remote Sens. Environ. 113 (9), 1868–1873. http://dx.doi.org/10.1016/j.rse.2009.04.006, URL: https://linkinghub.elsevier.com/retrieve/pii/S0034425709001291.

Kasischke, E.S., Smith, K.B., Bourgeau-Chavez, L.L., Romanowicz, E.A., Brunzell, S., Richardson, C.J., 2003. Effects of seasonal hydrologic patterns in south Florida wetlands on radar backscatter measured from ERS-2 SAR imagery. Remote Sens. Environ. 88 (4), 423–441. http://dx.doi.org/10.1016/j.rse.2003.08.016, URL: https://linkinghub.elsevier.com/retrieve/pii/S0034425703002517.

Kim, J.-W., Lu, Z., Gutenberg, L., Zhu, Z., 2017. Characterizing hydrologic changes of the Great Dismal Swamp using SAR/InSAR. Remote Sens. Environ. 198, 187–202. http://dx.doi.org/10.1016/j.rse.2017.06.009, URL: https://linkinghub.elsevier.com/retrieve/pii/S0034425717302687.

Lang, M.W., Kasischke, E.S., 2008. Using C-Band synthetic aperture radar data to monitor forested wetland hydrology in Maryland's Coastal Plain, USA. IEEE Trans. Geosci. Remote Sens. 46 (2), 535–546. http://dx.doi.org/10.1109/TGRS.2007.909950, URL: http://ieeexplore.ieee.org/document/4407740/.

Lees, K., Artz, R., Chandler, D., Aspinall, T., Boulton, C., Buxton, J., Cowie, N., Lenton, T., 2021. Using remote sensing to assess peatland resilience by estimating soil surface moisture and drought recovery. Sci. Total Environ. 761, 143312. http://dx.doi.org/10.1016/j.scitotenv.2020.143312, URL: https://linkinghub.elsevier.com/retrieve/pii/S0048969720368431.

Mackin, F., Barr, A., Rath, P., Eakin, M., Jeffrey, R., Valverde, F.F., Ryan, J., 2017. Best Practice in Raised Bog Restoration in Ireland. Technical Report 99, National Parks and Wildlife Service, Department of Culture, Heritage and the Gaeltacht, Ireland, p. 82.

Millard, K., Richardson, M., 2018. Quantifying the relative contributions of vegetation and soil moisture conditions to polarimetric C-Band SAR response in a temperate peatland. Remote Sens. Environ. 206, 123–138. http://dx.doi.org/10.1016/j.rse.2017.12.011, URL: https://linkinghub.elsevier.com/retrieve/pii/S0034425717305862.

Mitsch, W.J., Gosselink, J.G., 2007. Wetlands, fourth ed. Wiley, Hoboken, N.J..

Monteverde, S., Healy, M., O'Leary, D., Daly, E., Callery, O., 2022. Management and rehabilitation of peatlands: The role of water chemistry, hydrology, policy, and emerging monitoring methods to ensure informed decision making. Ecol. Inform. 69, 101638. http://dx.doi.org/10.1016/j.ecoinf.2022.101638, URL: https://linkinghub.elsevier.com/retrieve/pii/S1574954122000875.

Pedregosa, F., Varoquaux, G., Gramfort, A., Michel, V., Thirion, B., Grisel, O., Blondel, M., Prettenhofer, P., Weiss, R., Dubourg, V., Vanderplas, J., Passos, A., Cournapeau, D., Brucher, M., Perrot, M., Duchesnay, E., 2011. Scikit-learn: Machine learning in Python. J. Mach. Learn. Res. 12, 2825–2830.

Planning, M., Consultants, E., 2022. Clooneeny Bog, Co Longford Decommissioning and Rehabilitation 2022. Technical Report, MKO, URL: https://www.bnmpcas.ie/wp-content/uploads/sites/18/2022/03/AASR-Clooneeny-F-020222-211019-1.pdf.

Price, J.S., McCarter, C.P., Quinton, W.L., 2023. Groundwater in Peat and Peatlands. The Groundwater Project, http://dx.doi.org/10.21083/978-1-77470-015-0, URL: http://gw-project.org/books/groundwater-in-peat-and-peatlands/.

Quinty, F., Rochefort, L., 2003. Peatland Restoration Guide, second ed. Canadian Sphagnum Peat Moss Association, St. Albert, AB, OCLC: 60833193.

Räsänen, A., Tolvanen, A., Kareksela, S., 2022. Monitoring peatland water table depth with optical and radar satellite imagery. Int. J. Appl. Earth Obs. Geoinf. 112, 102866. http://dx.doi.org/10.1016/j.jag.2022.102866, URL: https://linkinghub.elsevier.com/retrieve/pii/S1569843222000681.

Regan, S., Swenson, M., O'Connor, M., Gill, L., 2020. Ecohydrology, Greenhouse Gas Dynamics and Restoration Guidelines for Degraded Raised Bogs. Technical Report 342, Environmental Protection Agency, Johnstown Castle, Co. Wexford.

Sass, G.Z., Creed, I.F., 2008. Characterizing hydrodynamics on boreal landscapes using archived synthetic aperture radar imagery. Hydrol. Process. 22 (11), 1687–1699. http://dx.doi.org/10.1002/hyp.6736, URL: https://onlinelibrary.wiley.com/doi/10.1002/hyp.6736.

Wagner, W., Lemoine, G., Borgeaud, M., Rott, H., 1999. A study of vegetation cover effects on ERS scatterometer data. IEEE Trans. Geosci. Remote Sens. 37 (2), 938–948. http://dx.doi.org/10.1109/36.752212, URL: http://ieeexplore.ieee.org/document/752212/.

Wang, Y., Hess, L.L., Filoso, S., Melack, J.M., 1995. Understanding the radar backscattering from flooded and nonflooded Amazonian forests: Results from canopy backscatter modeling. Remote Sens. Environ. 54 (3), 324–332. http://dx.doi.org/10.1016/0034-4257(95)00140-9, URL: https://linkinghub.elsevier.com/retrieve/pii/0034425795001409.

Worrall, F., Armstrong, A., Holden, J., 2007. Short-term impact of peat drain-blocking on water colour, dissolved organic carbon concentration, and water table depth. J. Hydrol. 337 (3–4), 315–325. http://dx.doi.org/10.1016/j.jhydrol.2007.01.046, URL: https://linkinghub.elsevier.com/retrieve/pii/S002216940700073X.

Zhang, B., Wdowinski, S., Gann, D., Hong, S.-H., Sah, J., 2022. Spatiotemporal variations of wetland backscatter: The role of water depth and vegetation characteristics in Sentinel-1 dual-polarization SAR observations. Remote Sens. Environ. 270, 112864. http://dx.doi.org/10.1016/j.rse.2021.112864, URL: https://linkinghub.elsevier.com/retrieve/pii/S0034425721005848.